[1]Mat Syai'in

Enhancing Power Flow Through Advanced Application of Extreme Learning Machine Generator Capability Curve

Journal of Electrical Systems

Abstract: - Power flow analysis is a key component in system evaluation. Among the various methods available, the Newton-Raphson approach is particularly effective. However, this method typically represents the generator capability curve (GCC) using a quadrilateral limit, defined by Pmin-Pmax and Qmin-Qmax constraints. This often results in certain parts of the GCC being disregarded, which can lead to less optimal performance during power flow analysis. To address this issue, this study introduces a new method: the Extreme Learning Machine Generator Capability Curve (ELMGCC), which aims to more accurately represent the shape of the GCC. ELMGCC replaces the traditional rectangular limits to better constrain the generator's operating point during power flow calculations. The study applies ELMGCC to both the Newton-Raphson (NR) and Fast Decoupled (FD) power flow methods to assess the effectiveness of this new approach. Simulation results using IEEE 30 Bus data with slight modifications show that the proposed method can maintain PV Bus performance up to 83.33% and reduce losses by 0.108216368053700 MW and 0.872096049537200 MVar for the NR method, and by 0.108236277781099 MW and 0.872099845833500 MVar for the FD method.

Keywords: Beta, Extreme Learning Machine (ELM), Generator Capability Curves (GCC), H-matrix, Newton-Raphson, Fast Decouple, Power Flow.

I. INTRODUCTION

Power flow stands as a pivotal component within the power system analysis, integral to both operational and planning phases. Its utilization serves the purpose of ascertaining the voltage magnitude and angle at each bus, along with computing active and reactive power, as well as identifying the losses incurred during power generation under specific load conditions[1][2].

Many methods have been suggested to improve the power flow process and speed up computational procedures. One notable approach is the optimally ordered and sparsity-oriented programming technique, first conceptualized by Tinney. Later, Brian Stott introduced the Newton-Raphson (NR)[3], decoupled, and fast decoupled methods. Although the NR method has relatively long computational times per iteration, it converges faster than other techniques. This characteristic has made the NR method standard in the industry[4].

Currently, as electrical systems evolve into more complex and extensive networks, Newton's foundational technique has been further developed and integrated with other methods to improve its performance in the power flow process. Power electronic elements, like converters, significantly influence power quality by introducing harmonics. The decoupled Newton's method accelerates the iteration process in converter model calculations[5]. Although Newton's basic techniques can address some power system issues, they are inadequate when generator operation is limited to rectangular constraints[6][7].

This study presents a technique for applying operational constraints on generators in power flow applications by using the Generator Capability Curve (GCC) model. To simplify the complex mathematical procedures involved in creating the GCC, we utilize the Extreme Learning Machine (ELM)[8][9] to replicate its shape. Furthermore, a security checking algorithm has been developed to facilitate the limit verification process.

The paper will proceed as follows in its discussion. Section II elaborates on the utilization of ELM to replicate GCC and its integration into power flow processes. This section covers the discussion on NR power flow, the method of mimicking GCC using ELM, and an explanation of how the security checking algorithm operates within NR power flow operations. Section III outlines the verification process of the proposed method using IEEE 30 bus test data. Finally, the conclusion is provided in Section IV.

II. METHODOLOGY

A. Newton Raphson Power Flow Overview

NR is frequently employed for addressing power flow dilemmas [10]. The following outlines the procedure for resolving power flow utilizing NR, relying on one-dimensional equations depicted in equation (1).

$$f(x) = c \tag{1}$$

[1] *Politeknik Perkapalan Negeri Surabaya (PPNS)/ Shipbuilding Institute of Polytechnic Surabaya (SHIPS), Indonesia
email : matt.syaiin@ppns.ac.id

The iterative procedure in NR employs equation:

$$x_i^{(k+1)} = x_i^{(k)} + \Delta x_i^{(k)} \quad (2)$$

$$\Delta x_i^{(k)} = \frac{\Delta c^k}{\left(\frac{df}{dx}\right)^k} \quad (3)$$

Subsequently, to address the power flow predicament, equations (1-3) mentioned earlier are employed. The model for the power flow equation can be expressed as described in equation (4) and (5).

$$P_i = \sum_{j=1}^{n} |V_i||V_j||Y_{ij}|cos(\theta_{ij} - \delta_i + \delta_j) \quad (4)$$

$$Q_i = \sum_{j=1}^{n} |V_i||V_j||Y_{ij}|sin(\theta_{ij} - \delta_i + \delta_j) \quad (5)$$

Based on equations (4) and (5) previously mentioned, there exist variables requiring optimization, specifically δ and |V|. Using equation (2) as a basis, the values of δ and |V| for each iteration can be incorporated into the subsequent equations (6-7).

$$\delta_i^{(k+1)} = \delta_i^{(k)} + \Delta\delta_i^{(k)} \quad (6)$$

$$|V|_i^{(k+1)} = |V|_i^{(k)} + \Delta|V|_i^{(k)} \quad (7)$$

In the meantime, equation (3) can be expressed as shown in equations (8-10).

$$\begin{bmatrix} \Delta\delta \\ \Delta|V| \end{bmatrix} = \begin{bmatrix} J_1 & J_2 \\ J_3 & J_4 \end{bmatrix}^{-1} \quad (8)$$

$$\Delta P_i^{(k)} = P_i^{(sch)} - P_i^{(k)} \quad (9)$$

$$\Delta Q_i^{(k)} = Q_i^{(sch)} - Q_i^{(k)} \quad (10)$$

The J matrix mentioned in equation (8) is alternatively referred to as the Jacobian matrix, directly associated with the PV-bus and PQ-bus. Both PV-bus and PQ-bus entail variables essential for optimization, specifically δ and Q for PV-bus, and δ and |V| for PQ-bus. Within the J matrix, these variables are divided into four components: J_1, J_2, J_3, and J_4. The equations for each of these components can be expressed in equations (11-18) as follows:

The equation of J_1

$$\frac{\partial P_i}{\partial \delta_i} = \sum_{j\neq 1} |V_i||V_j||Y_{ij}|sin(\theta_{ij} - \delta_i + \delta_j) \quad (11)$$

$$\frac{\partial P_i}{\partial \delta_j} = -|V_i||V_j||Y_{ij}|sin(\theta_{ij} - \delta_i + \delta_j) \quad j\neq 1 \quad (12)$$

The equation of J_2

$$\frac{\partial P_i}{\partial |V|_i} = 2|V_i||Y_{ii}|cos_{ii} + \sum_{j\neq 1} |V_j||Y_{ij}|cos(\theta_{ij} - \delta_i + \delta_j) \quad (13)$$

$$\frac{\partial P_i}{\partial |V|_j} = -|V_i||Y_{ij}|cos(\theta_{ij} - \delta_i + \delta_j) \quad j\neq 1 \quad (14)$$

The equation of J_3

$$\frac{\partial Q_i}{\partial \delta_i} = \sum_{j\neq 1} |V_i||V_j||Y_{ij}|cos(\theta_{ij} - \delta_i + \delta_j) \quad (15)$$

$$\frac{\partial Q_i}{\partial \delta_j} = -|V_i||Y_{ij}|cos(\theta_{ij} - \delta_i + \delta_j) \quad j\neq 1 \quad (16)$$

The equation of J_4

$$\frac{\partial Q_i}{\partial |V|_i} = -2|V_i||Y_{ii}|sin_{ii} \quad + \sum_{j \neq 1} |V_j||Y_{ij}|sin(\theta_{ij} - \delta_i + \delta_j) \tag{17}$$

$$\frac{\partial Q_i}{\partial |V|_j} = -|V_i||Y_{ij}|sin(\theta_{ij} - \delta_i + \delta_j) \quad j \neq 1 \tag{18}$$

During every iteration, it's crucial to examine the P and Q values to determine if they remain within the specified limits. If during the iteration process, P and Q exceed the maximum limit, they are adjusted to the maximum condition. Conversely, if they fall below the minimum limit, they are adjusted accordingly. Figure 1 illustrates a flowchart of the NR algorithm, which includes a step for verifying the minimum and maximum limits for P and Q values.

The procedure for verifying the limits of P and Q depicted in the flowchart still employs a rectangular limit approach. Rectangular-shaped limits for P and Q are commonly utilized across various power flow algorithms [10][11]. While some commercial software[12] adopts a limit line method that conforms to the shape of the generator capability curve (GCC), which typically yields more accurate outcomes compared to using rectangular-shaped limits for P and Q. However, integrating GCC based limit methods into power flow can be quite intricate. This proposed approach introduces a straightforward algorithm to incorporate GCC limits into power flow using ELM (Extreme Learning Machine). Further elaboration on this process will be provided in the subsequent subsection.

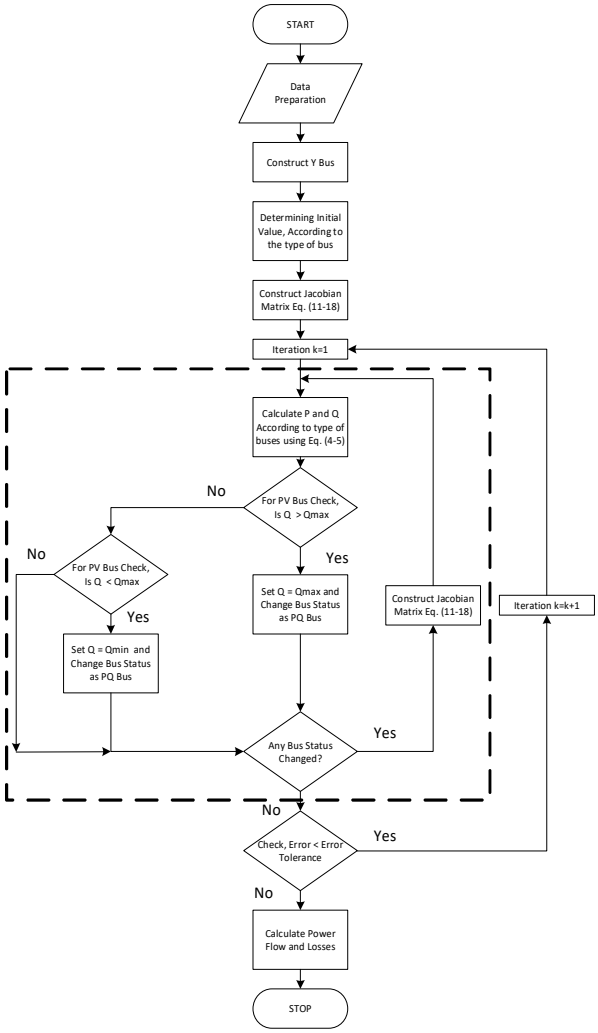

Figure 1. NR power flow diagram

B. GCC limit development using extreme learning machine (ELM)

As shown in Figure 2, the ELM neural network (NN) model described in this paper consists of only one input and output, as well as a single hidden layer. This hidden layer employs a total of 27 neurons. The objective of the ELM training procedure is to obtain the beta values. The data utilized in this paper employs a sampling point from

the GCC data obtained from the generator datasheet. To streamline the intricate computational process, the GCC axes are transformed into polar coordinates, represented as theta (θ) and Magnitude (R), as depicted in Figure 3.

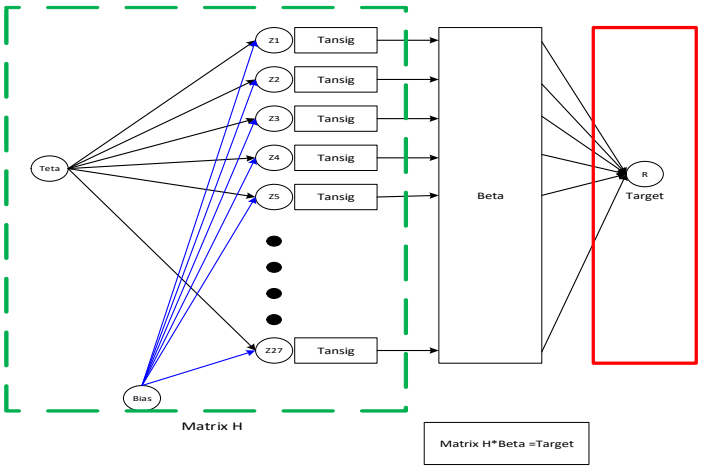

Figure 2. GCC using the ELM model

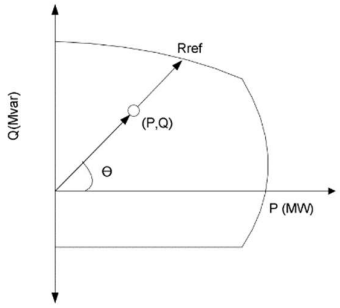

Figure 3. Relationship between P, Q, θ, R and Rref

Once the angle θ is established, the length of R can be computed. Thus, in the ELM model outlined in this paper, θ serves as the input, while R becomes the output of the ELM. Subsequently, both input and output data undergo training to derive the beta values, which represent the relationship between θ and R. The ELM training process essentially involves multiplying the inverse matrix of H and T (target). Once the beta values are determined, they are utilized to generate the digital GCC, referred to as ELMGCC (Extreme Learning Machine Generator Capability Curve). The GCC utilized in this paper is adapted from reference [13] with slight modifications. A total of 130 sampling points along the curves are utilized to reconstruct the GCC. The comparison between ELMGCC and the GCC datasheet is illustrated in Figure 4 below.

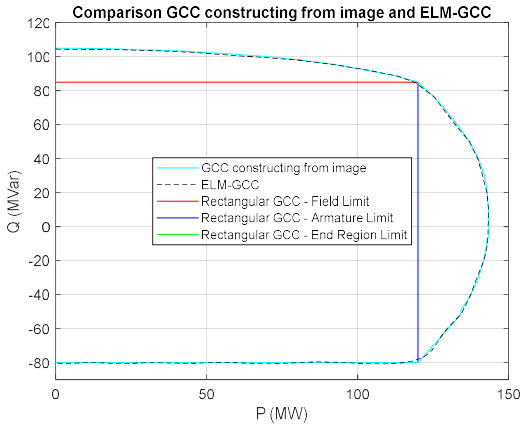

Figure 4. Comparison between GCC datasheet and ELMGCC

C. *Development of security checking algorithm*

The security checks outlined in this section utilize the output derived from ELMGCC, which can serve as a reference limit, as indicated in reference [13]. The security checking algorithm consists of three steps as follows: First, convert the values of P and Q into polar coordinates (θ, R). Second, utilize the angle θ to determine R or the distance to the original GCC line point Rref, as illustrated in Figure 3. Third, verify the safe operating condition of the generator by comparing the values of R and Rref. If R < Rref, then the values of P and Q remain within safe limits; otherwise, the Rref value and angle θ are immediately locked, as demonstrated in Figure 5.

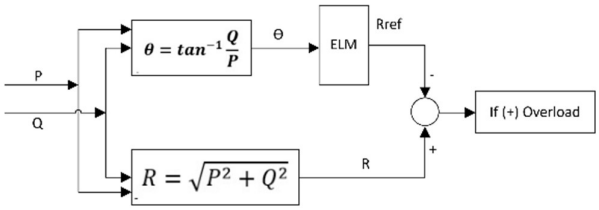

Figure 5. The security checks algorithm of the proposed method

D. *GCC Limit construct by ELM for improving performance NR power flow algorithm*

As illustrated in Figure 6, the proposed approach enhances the traditional P-Q limit representation by transitioning from a rectangular form to one based on ELMGCC. This method simplifies the process of determining realistic Generator Capability Curve (GCC) shapes by avoiding complex mathematical equations and providing greater adaptability to various curve forms. The ELMGCC is then integrated into the Newton-Raphson (NR) power flow algorithm, as shown in Figure 7. While the overall flowchart of the enhanced NR power flow algorithm remains similar to the one described in Figure 1, the key difference lies in how generator operating boundaries are enforced. The proposed method replaces conventional fixed limits with ELMGCC and incorporates a security checking algorithm to verify safe operating conditions.

The integration of the ELMGCC-based security check ensures safe and efficient generator operation within its capability curve limits. The iterative process begins with the calculation of power mismatches (ΔP and ΔQ) and the verification of generator reactive power (Q) limits using the ELM model, which predicts Qmin and Qmax based on the current active power (P). If the reactive power exceeds its limits, the bus type is dynamically converted from PV to PQ, relaxing voltage magnitude regulation. To further ensure safe operation, the security check converts the P-Q values into polar coordinates (θ, R), calculates the distance (R) to the reference GCC limit (Rref), and compares the values. If R < Rref, the generator is deemed to operate safely; otherwise, the values of θ and Rref are locked to prevent violations.

The NR algorithm iteratively updates the bus voltages, recalculates mismatches, and checks for convergence. This integrated approach not only enhances the accuracy and computational efficiency of power flow analysis but also ensures that generator operation consistently adheres to its physical and thermal constraints.

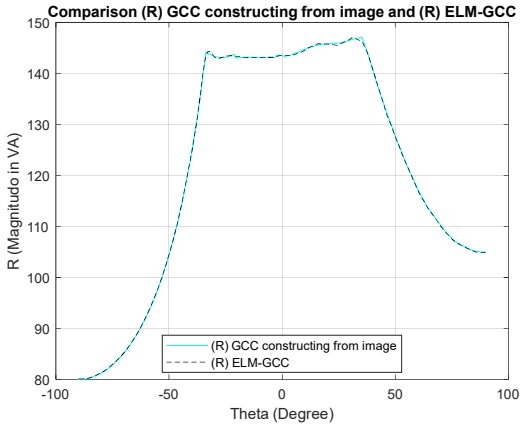

Figure 6. Comparison of R datasheet values with R results obtained from ELMGCC

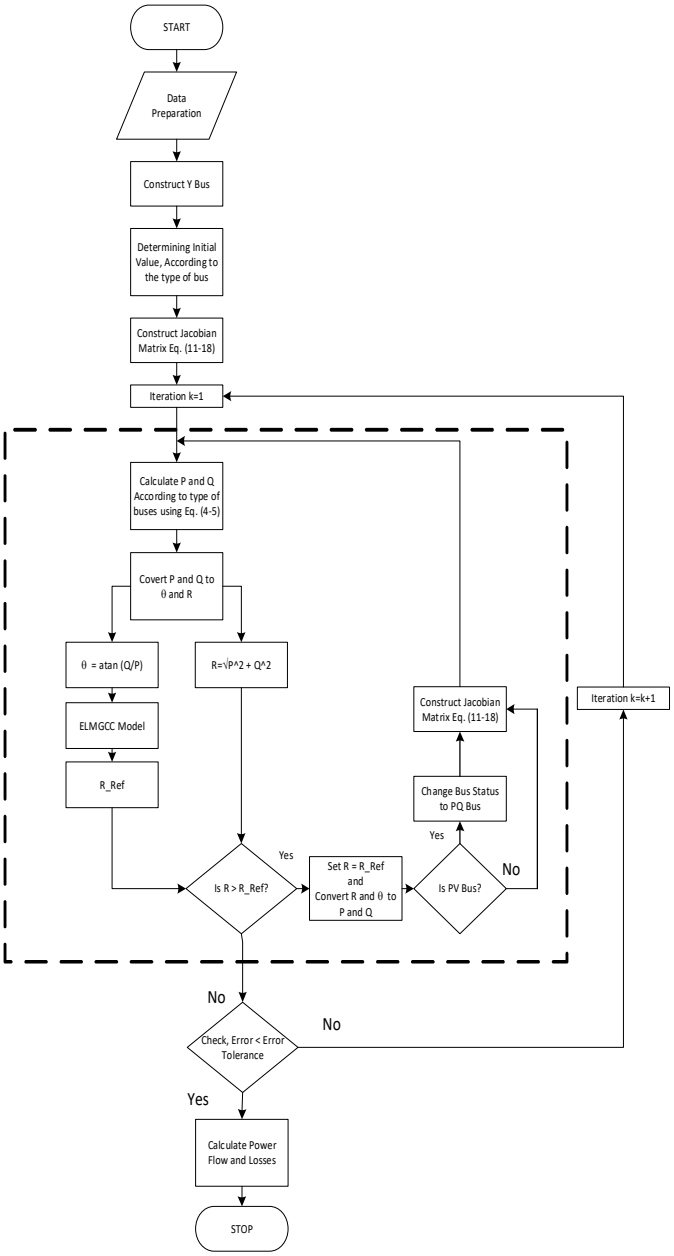

Figure 7. Flowchart of the NR power flow enhancement algorithm utilizing ELMGCC

III. SIMULATION RESULTS AND ANALYSIS

A. Simulation Data

In this study, we use IEEE 30 bus data with minor adjustments to the load data to showcase the effectiveness of the proposed method in handling load variations compared to the rectangular GCC approach. The specific modifications involve adjusting the reactive load data as follows: bus 3 from 1.2 MVar to 11.2 MVar, bus 4 from 1.6 MVar to 11.6 MVar, and bus 11 from 0 MVar to 32 MVar. These adjustments are described in three different cases:

Case 1: Ignoring the GCC limit

Case 2: Applying the Rectangular GCC to the NR Power Flow and FD Power Flow

Case 3: Applying the ELMGCC to the NR Power Flow and FD Power Flow

The GCC data, sourced from reference [13], has been slightly modified to assess the effectiveness of the proposed method

B. ELMGCC (Extreme Learning Machine Generator Capability Curve)

The ELM framework utilized for modelling GCC comprises a single input and output. The input data for ELM consists of angles ranging from -90 to +90, while the output data represents R-values, indicating the magnitude of complex power. GCC, obtained from datasheets or images, is segmented into a minimum of 130 pairs (P, Q), which serve as the training data for ELM. The complete stages of the training process can be delineated as follows:

Step 1: Data Preparation. Training data is prepared by converting pair data (P, Q) into angle θ and R data.

Step 2: Construction of H-Matrix. The H-Matrix is constructed to match the number of input data and the number of neurons in the hidden layer. With 130 input data points and 27 neurons in the hidden layer, the size of the H-Matrix is 130x27.

Step 3: Selection of Activation Function and Weights. The activation function and weights for the hidden and bias layers are determined. Weight values can be generated randomly, ensuring that the resulting H-Matrix is non-singular. The Tanh-Sigmoid (Tansig) activation function is utilized in this study. Generally, the equations used to formulate the H-Matrix, as shown in (19) are as follows:

$$H = \begin{bmatrix} Z_{1_1} & Z_{1_2} & Z_{1_3} & \cdots & \cdots & Z_{1_{27}} \\ Z_{2_1} & Z_{2_2} & Z_{2_3} & \cdots & \cdots & Z_{2_{27}} \\ \vdots & \vdots & \vdots & \cdots & \cdots & \vdots \\ Z_{130_1} & Z_{130_2} & Z_{130_3} & \cdots & \cdots & Z_{130_{27}} \end{bmatrix} \quad (19)$$

With,

$$Z_{1_1} = tansig\big(\theta(1,1) * w(1,1) + b(1,1)\big)$$
$$Z_{1_2} = tansig\big(\theta(1,1) * w(1,2) + b(1,2)\big)$$
$$Z_{1_3} = tansig\big(\theta(1,1) * w(1,3) + b(1,3)\big)$$
$$\vdots \quad \vdots \quad \vdots$$
$$Z_{2_3} = tansig\big(\theta(2,1) * w(2,3) + b(2,3)\big)$$
$$\vdots \quad \vdots \quad \vdots$$
$$Z_{30_{27}} = tansig\big(\theta(130,1) * w(130,27) + b(130,27)\big)$$

Step 4: The computation of Beta (β) involves taking the inverse of the H-Matrix. This process yields the value of Beta. The equations (20-22) utilized for this purpose is described in reference [14].

$$H\beta = T \quad (20)$$

$$\beta = H^{-1}T \quad (21)$$

$$\beta = \left(\frac{I}{C} + H^T H\right)^{-1} H^T T \quad (22)$$

Step 5: The integration of Beta and the H-Matrix into the NR power flow algorithm is carried out. The comparison between the target data and the results obtained from ELM is illustrated in Figure 6. From the figure, R can be represented as a Generator Capability Curve by converting it into P and Q as shown in Figure 5, with the results displayed in Figure 4. The step-by-step algorithm for power flow using ELMGCC as the generator capability constraint is illustrated in Figure 7.

C. Result and Analysis

The analysis in this study covers the following aspects:

- Assessing the voltage magnitude and angle at each bus due to load variations.
- Evaluating the generator's ability to manage specific voltage levels on PV Buses.
- Analysing system losses and the convergence process.

1) Assessing the voltage magnitude and angle at each bus due to load variations

From Table 1, it can be observed that the results of power flow analysis using the Newton-Raphson (NR) method, and the Fast Decoupled (FD) method are highly consistent. To highlight differences between the methods, the results

are presented with eight decimal places, as the values up to five decimal places are identical. In this study, NR and FD power flow methods were evaluated under three different constraint conditions, particularly concerning the GCC limits: the first condition is the rectangular limit of the GCC, the second is the ELMGCC limit, and the third is without any limits.

According to the data in Table 1, the NR and FD power flow methods yielded the best voltage magnitude results when considering no limits, ELMGCC limits, and rectangular GCC limits, respectively. The voltage magnitude is influenced by the reactive power (Q) capacity provided by the generators. Therefore, to verify the operating point of each generator, it is necessary to plot these points according to the GCC constraints.

In the IEEE 30 Bus system simulated in this study, there are six generators: Generator Bus 1 operates as the Slack Bus, and Generator Buses 2, 5, 8, 11, and 13. The operating points of all these generators are shown in Figure 8.

Table 1: Comparison of voltage levels across each bus

No	Bus Status	Generator Setting Voltage (Bus)	Rectangular GCC Limit		ELMGCC Limit (Proposed Method)		No GCC limit	
			NR Power Flow |V| (pu)	FD Power Flow |V| (pu)	NR Power Flow |V| (pu)	FD Power Flow |V| (pu)	NR Power Flow |V| (pu)	FD Power Flow |V| (pu)
1	Slack	1.060	1.06000000	1.06000000	1.06000000	1.06000000	1.06000000	1.06000000
2	PV	1.043	1.04127102	1.04127096	1.04300000	1.04300000	1.04300000	1.04300000
3	PQ		1.01005365	1.01005371	1.01265658	1.01265661	1.01452680	1.01452680
4	PQ		1.00259712	1.00259720	1.00573621	1.00573624	1.00799211	1.00799210
5	PV	1.010	1.01000000	1.01000000	1.01000000	1.01000000	1.01000000	1.01000000
6	PQ		1.00389120	1.00389121	1.00791615	1.00791606	1.01065516	1.01065516
7	PQ		0.99857241	0.99857243	1.00097496	1.00097491	1.00260953	1.00260954
8	PV	1.010	1.00554123	1.00554124	1.01000000	1.01000000	1.01000000	1.01000000
9	PQ		1.01809582	1.01809561	1.02897807	1.02897756	1.05021202	1.05021203
10	PQ		1.02128637	1.02128606	1.02917765	1.02917692	1.04332728	1.04332730
11	PV	1.082	1.00563320	1.00563299	1.02892843	1.02892791	1.08200000	1.08200000
12	PQ		1.04869547	1.04869571	1.05172975	1.05173011	1.05614372	1.05614369
13	PV	1.071	1.07100000	1.07100000	1.07100000	1.07100000	1.07100000	1.07100000
14	PQ		1.03200666	1.03201399	1.03566477	1.03567741	1.04124195	1.04124102
15	PQ		1.02569242	1.02568968	1.02990230	1.02989751	1.03652001	1.03652030
16	PQ		1.02981364	1.02981361	1.03492407	1.03492389	1.04348595	1.04348594
17	PQ		1.01843915	1.01843891	1.02552194	1.02552136	1.03803665	1.03803666
18	PQ		1.01178490	1.01178312	1.01736110	1.01735792	1.02674641	1.02674660
19	PQ		1.00673749	1.00673623	1.01310700	1.01310469	1.02410595	1.02410609
20	PQ		1.00958341	1.00958241	1.01633599	1.01633411	1.02812599	1.02812609
21	PQ		1.00975079	1.00975035	1.01743919	1.01743831	1.03101725	1.03101727
22	PQ		1.01065855	1.01065809	1.01824781	1.01824686	1.03158425	1.03158428
23	PQ		1.01249842	1.01249654	1.01768038	1.01767707	1.02595600	1.02595619
24	PQ		1.00342964	1.00342881	1.00986845	1.00986692	1.02029378	1.02029386
25	PQ		1.00396045	1.00396016	1.00971234	1.00971153	1.01728004	1.01728006
26	PQ		0.98603820	0.98603757	0.99189626	0.99189609	0.99960172	0.99960161
27	PQ		1.01299982	1.01299982	1.01827164	1.01827120	1.02399047	1.02399047
28	PQ		1.00283170	1.00283171	1.00710336	1.00710324	1.00964977	1.00964978
29	PQ		0.99293791	0.99293823	0.99832507	0.99832472	1.00416745	1.00416746
30	PQ		0.98133529	0.98133574	0.98678869	0.98678838	0.99270204	0.99270205

2) Evaluating the generator's ability to manage specific voltage levels on PV Buses.

The operating point of each generator in maintaining the voltage magnitude of the PV buses is illustrated in Figure 8. Figure 8 illustrates that the operating points of generators vary across different methods and constraints, with some points falling within the GCC and others outside of it. Operating points outside the GCC indicate that those settings cannot be implemented in real systems. As shown in Figure 8, the proposed method demonstrates a better ability to handle load variations while maintaining the voltage magnitude of PV buses, with results that are feasible for real-world application.

For clarity, the discussion begins with Generator Bus 11, depicted in Figure 9, which shows significant differences among the constraints. Figure 9 presents three types of operating points, with the NR and FD power flow methods yielding similar results. However, the constraints lead to significantly different outcomes.

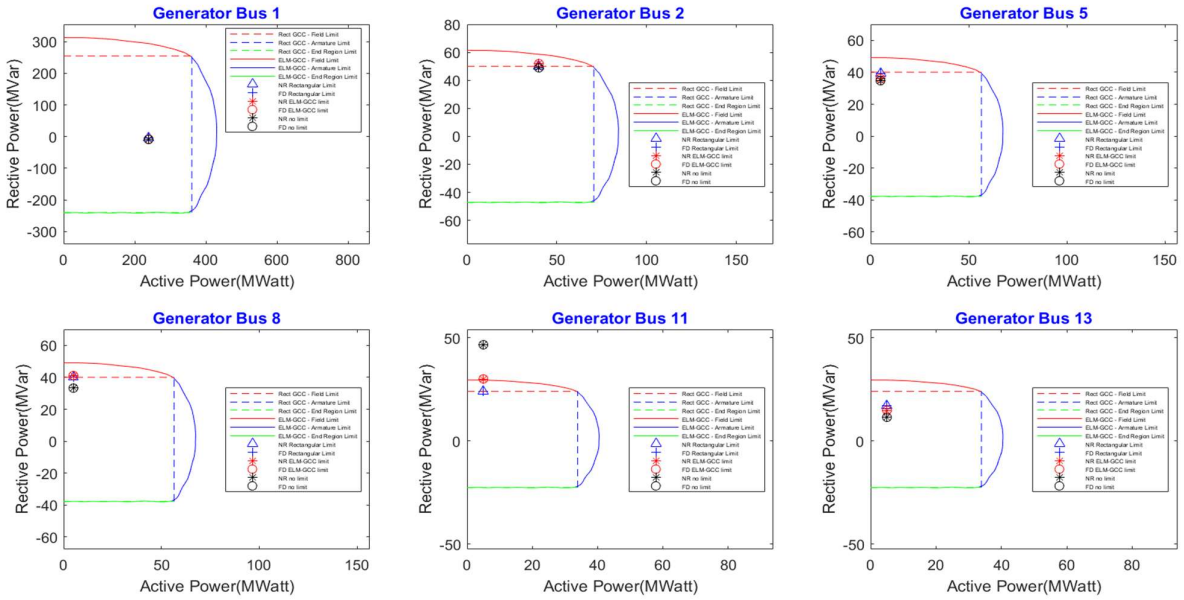

Figure 8. Operating point of the generator

Under the first constraint, where there are no limits, the operating points fall outside both the rectangular GCC and ELMGCC boundaries. This condition is not viable in real systems because the generator's capability to supply reactive power (Q) is exceeded, even though the resulting voltage magnitude aligns with the PV bus voltage level.

Under the second constraint, the operating point of Generator Bus 11 lies on the boundary of the rectangular GCC. While this operating point is generally good, some reactive power remains unused in maintaining the voltage magnitude. This scenario is feasible for real systems, but there is a significant difference in the voltage magnitudes produced by the NR and FD power flow methods due to the unused reactive power capacity.

For the third constraint, the operating point of Generator Bus 11 is positioned on the ELMGCC line at the maximum limit, meaning that the entire capacity of reactive power is used to maintain the voltage magnitude. This condition can still be implemented in real systems. Therefore, the proposed method has proven to have good capability in maintaining the voltage magnitude on PV buses.

In Figure 9, the voltage magnitude of PV Bus 11 is set to 1.082 pu, which requires the generator to supply 46.5588848935631 Mvar. However, the generator's capacity is only 30 Mvar under the ELMGCC constraint and 24 Mvar under the rectangular GCC limit. This indicates that achieving the desired voltage magnitude at PV Bus 11 is not feasible in a real system due to insufficient reactive power supply.

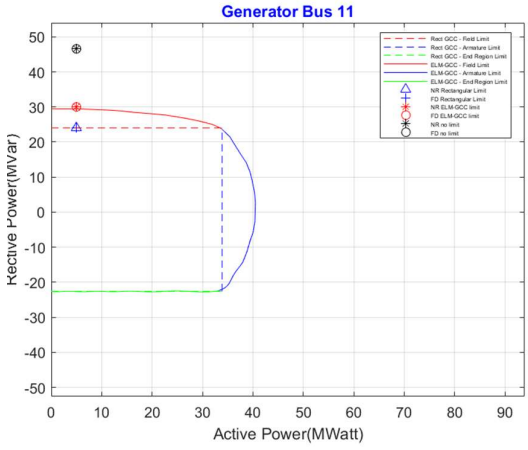

Figure 9. Operating point of Generator Bus 11

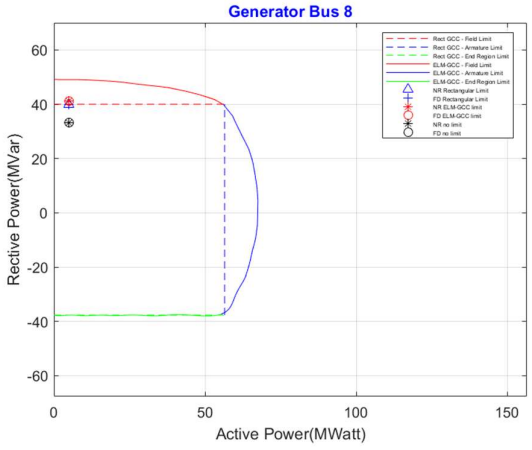

Figure 10. Operating point of Generator Bus 8 under three different scenarios

Under the ELMGCC constraint with a 30 Mvar generator capacity, the voltage magnitude at Bus 11 is 1.02892843 pu with the NR power flow method and 1.02892791 pu with the FD power flow method. In contrast, under the rectangular GCC limit with a 24 Mvar generator capacity, the voltage magnitude is 1.00563320 pu with the NR power flow method and 1.00563299 pu with the FD power flow method. This means the proposed method is better than the rectangular constraint by 0.022640282 (2.2640282%) for NR power flow and 0.022639995 (2.2639995%) for FD power flow.

Figure 10 depicts the operating point for Generator Bus 8. The figure shows that the operating point under the ELMGCC constraint is slightly higher than under the rectangular GCC constraint. The voltage magnitude at Bus 8 is set to 1.01000000 pu. For the ELMGCC limit, both the NR power flow and FD power flow methods yield a voltage magnitude of 1.01000000 pu. In contrast, with the rectangular GCC limit, the NR power flow results in a voltage magnitude of 1.00554123 pu, and the FD power flow results in 1.00554124 pu. The rectangular GCC limit fails to achieve the desired voltage magnitude at the PV bus because the reactive power supply is insufficient. To maintain the voltage magnitude, 41.1404586546978 MVar is needed for NR power flow and 41.1406771731229 MVar for FD power flow, while the rectangular GCC limit is set to a maximum of 40 MVar. Consequently, the voltage decreases by 0.00445877 pu (0.445877%) for NR power flow and by 0.00445876 pu (0.445876%) for FD power flow.

Figure 11 displays the operating point for Generator Bus 2. It shows that the operating point under the ELMGCC constraint falls within the ELMGCC boundaries, whereas the operating point under the rectangular GCC constraint falls outside its boundaries.

The voltage magnitude at Bus 2 is set at 1.04300000 pu. For the ELMGCC limit, both the NR power flow and FD power flow methods achieve this voltage magnitude. However, with the rectangular GCC constraint, the NR power flow yields a voltage of 1.04127102 pu, and the FD power flow yields 1.04127096 pu. The rectangular GCC limit does not reach the desired voltage magnitude at the PV bus due to inadequate reactive power supply. To maintain the voltage magnitude, 51.8728625803658 MVar is needed for NR power flow and 51.8728858950415 MVar for FD power flow, while the rectangular GCC limit is capped at 50 MVar. As a result, the voltage decreases by 0.00172898 pu (0.172898%) for NR power flow and 0.00172904 pu (0.172904%) for FD power flow. The differences in the operating points of Generator Bus 2 are depicted in Figure 12.

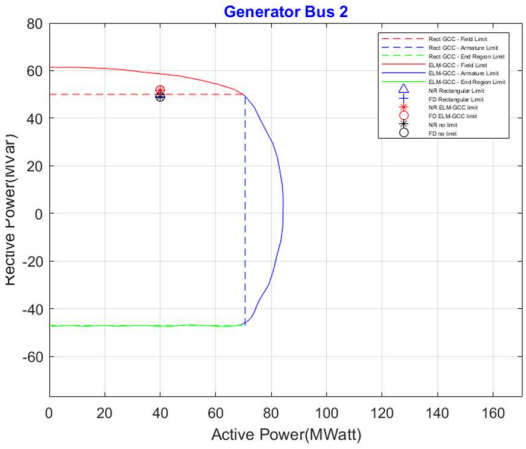

Figure 11. Operating point of Generator Bus 2 across three different cases

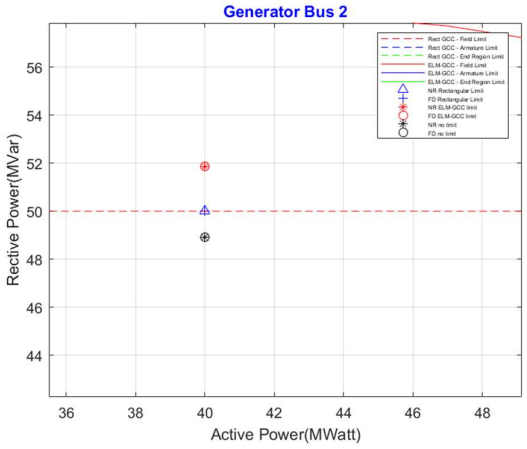

Figure 12. Detailed view of the operating point for Generator Bus 2 under three different cases

3) Analyzing system losses and the convergence process

Table 2 shows the losses associated with different methods and constraints. According to the table, the minimum losses are observed with the NR and FD methods under the no-limit GCC constraint. Although these methods result in the lowest losses compared to others, the operating points for the generators, particularly Generator Bus 11, are not feasible for real-world systems because they fall outside the generator's capacity.

The NR and FD methods with the rectangular GCC limit incur higher losses compared to other constraints. This is due to the generator's setting using a straight line, which does not accurately represent the realistic GCC. The GCC model used in this research, adapted from reference [13], includes various circular lines to represent Field Limit, Armature Limit, and End-of-Region Limit. This model adheres to the ELMGCC limit. The advantage of the ELMGCC limit is its ability to utilize the entire area within the GCC to minimize losses, unlike the rectangular GCC, which only represents the GCC with a rectangular shape and therefore leaves some areas underutilized for loss reduction.

Table 2: Losses among methods and constraints

No	Methods and Constraints	Losses	
		P(MW)	Q(MVar)
1	NR with constraint rectangular GCC limit	15.476358633950	14.023520268011
2	FD with constraint rectangular GCC limit	15.476423979388	14.023579978496
3	NR with constraint ELMGCC limit	15.368142265897	13.151424218473
4	FD with constraint ELMGCC limit	15.368187701607	13.151480132662
5	NR with constraint no GCC limit	15.251826476375	13.040475652831
6	FD with constraint no GCC limit	15.251809153382	13.040479246052

As a result, the proposed method can reduce losses by 0.108216368053700 MW and 0.872096049537200 MVar for the NR method, and by 0.108236277781099 MW and 0.872099845833500 MVar for the FD method. The detailed analysis of the results underscores that the proposed ELMGCC method achieves an effective balance between minimizing system losses and maintaining operational feasibility. Its capability to enable flexible and efficient use of reactive power within realistic GCC boundaries gives it a clear advantage over traditional rectangular constraints. Additionally, the consistency observed between the NR and FD methods highlights the robustness and reliability of the simulation framework employed. These findings offer significant insights for improving voltage and reactive power management in power systems, particularly under diverse operational conditions. Future research could focus on evaluating the scalability of the ELMGCC method for larger, more complex systems and exploring its integration with advanced optimization techniques to enhance its performance and applicability further.

D. Limitations

This study has some limitations that warrant further consideration and could form the basis for future research. The analysis was conducted on the simplified IEEE 30-Bus system, which may not fully capture the intricacies and challenges of real-world power grids with more diverse load and network dynamics. Additionally, the study did not include transient stability or dynamic load variation analyses, which are critical for understanding their potential impact on voltage profiles and system losses. Although the ELMGCC model showed improved utilization of generator reactive power capacity, it did not account for potential thermal or mechanical constraints that could arise during prolonged operation at maximum reactive power levels. The study primarily focused on evaluating the convergence of the Newton-Raphson (NR) and Fast Decoupled (FD) methods without addressing their computational efficiency in larger systems or under extreme loading scenarios. Furthermore, external factors such as market fluctuations, renewable energy integration, and environmental policies were excluded from the analysis, which may limit the practical relevance of the proposed method in contemporary, evolving power grid scenarios. Future studies are encouraged to expand the application of the ELMGCC method to more complex systems, incorporate transient and dynamic load analyses, and explore its integration with renewable energy sources to assess its scalability and adaptability. Advanced optimization approaches, including machine learning and metaheuristic algorithms, could further improve the computational efficiency and precision of the proposed method. Moreover, incorporating economic and environmental considerations, as well as validating the model through laboratory-scale experiments or hardware-in-the-loop simulations, would provide deeper insights into the practical implementation of the ELMGCC model for reactive power management and voltage control in modern power systems.

IV. CONCLUSION

In the first evaluation, which involves assessing the voltage magnitude and angle at each bus due to load variation, the results show that using a constraint that ignores the GCC limit allows the predetermined voltage levels at PV Buses to be fully achieved (100%). With the Rectangular GCC constraint, the achievable voltage levels at PV Buses are only 50%, applicable to Bus 1, 5, and 13. The ELMGCC constraint allows achieving 83.33% of the voltage levels at PV Buses, applicable to Bus 1, 2, 5, 8, and 13.

In the second evaluation, which examines the generator's ability to manage specific voltage levels on PV Buses, it is shown that using a constraint that ignores the GCC limit results in the operating point of the generator at Bus 11 exceeding the generator's capacity. This makes all results obtained with this constraint infeasible for real systems. In contrast, the Rectangular GCC and ELMGCC constraints ensure that the generator's operating points are applicable in real systems, although there is a change in the status of Bus, with PV buses becoming PQ buses is 50% for the Rectangular GCC constraint, and 17% for the ELMGCC constraint.

In the third evaluation, which focuses on system losses and the convergence process, both the NR and FD power flow methods exhibit good convergence across the three constraints, with results matching up to the fifth decimal place.

The proposed method, using the ELMGCC constraint, shows a significant improvement in reducing losses. It achieves a reduction of 0.108216 MW and 0.872096 MVar for the NR method, and 0.108236 MW and 0.872099 MVar for the FD method, compared to the Rectangular GCC constraint.

ACKNOWLEDGMENT

Thank you to the Ministry of Higher Education, Science, and Technology of the Republic of Indonesia for funding this research, facilitated through the Director of Politeknik Perkapalan Negeri Surabaya (PPNS) / Shipbuilding Institute of Polytechnic Surabaya (SHIPS), Indonesia.

REFERENCES

[1] S. Mouassa, A. Alateeq, A. Alassaf, R. Bayindir, I. Alsaleh, and F. Jurado, "Optimal Power Flow Analysis with Renewable Energy Resource Uncertainty Using Dwarf Mongoose Optimizer: Case of ADRAR Isolated Electrical Network," *IEEE Access*, vol. 12, pp. 10202–10218, 2024, doi: 10.1109/ACCESS.2024.3351721.

[2] Z. Fan, Z. Yang, J. Yu, K. Xie, and G. Yang, "Minimize Linearization Error of Power Flow Model Based on Optimal Selection of Variable Space," *IEEE Transactions on Power Systems*, vol. 36, no. 2, pp. 1130–1140, Mar. 2021, doi: 10.1109/TPWRS.2020.3012894.

[3] Z. Liu *et al.*, "Further Results on Newton-Raphson Method in Feasible Power-Flow for DC Distribution Networks," *IEEE Transactions on Power Delivery*, vol. 37, no. 2, pp. 1348–1351, Apr. 2022, doi: 10.1109/TPWRD.2021.3080132.

[4] M. Tostado-Veliz, S. Kamel, and F. Jurado, "Two Efficient and Reliable Power-Flow Methods with Seventh Order of Convergence," *IEEE Syst J*, vol. 15, no. 1, pp. 1026–1035, Mar. 2021, doi: 10.1109/JSYST.2020.3004667.

[5] A. Garces, "On the convergence of Newton's method in power flow studies for dc microgrids," *IEEE Transactions on Power Systems*, vol. 33, no. 5, pp. 5770–5777, Sep. 2018, doi: 10.1109/TPWRS.2018.2820430.

[6] Institute of Electrical and Electronics Engineers, *North American Power Symposium (NAPS), 2014: Date 7-9 Sept. 2014.*

[7] B. Park, L. Tang, M. C. Ferris, and C. L. Demarco, "Examination of Three Different ACOPF Formulations with Generator Capability Curves," *IEEE Transactions on Power Systems*, vol. 32, no. 4, pp. 2913–2923, Jul. 2017, doi: 10.1109/TPWRS.2016.2626142.

[8] H. D. P. De Carvalho, R. Fagundes, and W. Santos, "Extreme Learning Machine Applied to Software Development Effort Estimation," *IEEE Access*, vol. 9, pp. 92676–92687, 2021, doi: 10.1109/ACCESS.2021.3091313.

[9] T. Hussain, S. M. Siniscalchi, H. L. S. Wang, Y. Tsao, V. M. Salerno, and W. H. Liao, "Ensemble hierarchical extreme learning machine for speech dereverberation," *IEEE Trans Cogn Dev Syst*, vol. 12, no. 4, pp. 744–758, Dec. 2020, doi: 10.1109/TCDS.2019.2953620.

[10] B. G. Risi, F. Riganti-Fulginei, and A. Laudani, "Modern Techniques for the Optimal Power Flow Problem: State of the Art," Sep. 01, 2022, *MDPI*. doi: 10.3390/en15176387.

[11] M. A. Salam, *Fundamentals of electrical power systems analysis*. Springer Singapore, 2020. doi: 10.1007/978-981-15-3212-2.

[12] "ETAP ® 14.0.0 Demo Getting Started," 2015. [Online]. Available: www.etap.com

[13] B. Park, L. Tang, M. C. Ferris, and C. L. Demarco, "Examination of Three Different ACOPF Formulations with Generator Capability Curves," *IEEE Transactions on Power Systems*, vol. 32, no. 4, pp. 2913–2923, Jul. 2017, doi: 10.1109/TPWRS.2016.2626142.

[14] E. Cambria *et al.*, "Extreme learning machines," *IEEE Intell Syst*, vol. 28, no. 6, pp. 30–59, 2013, doi: 10.1109/MIS.2013.140.